MEMOIRS OF THE COLLEGE OF SCIENCE, University of Kyoto, Series A,
Vol. XXVIII, No. 4, Article 5, 1958

AN ELECTROMAGNETIC ISOTOPE SEPARATOR

BY

Jiro MUTO and Kotoyuki OKANO

(Received February 6, 1958)

ABSTRACT

In Kyoto University an electromagnetic isotope separator was constructed and has been in operation since September 1956. This article contains the description of main features of this machine and the discussions of experiments made on ion source efficiency as well as on the resolving power, together with some description of the separation of isotopes of neon, magnesium and silicon.

1. Introduction

Before the Second World War, it was very rare that the separated stable isotopes were applied in scientific researches. After the War, however, the isotopically pure or enriched samples have been employed in many scientific researches, because of the technical development of isotope separation acquired in the uranium separation project in U. S. A.

Nowadays, large isotope separating machines of production type which have the ion current of the order of 100 mA are in operation at the Oak Ridge National Laboratory in U. S. A. and at the Harwell Atomic Energy Research Establishment in England. In other European countries, i. e., France, Denmark, Sweden and others, comparatively small machines are constructed and in operation aiming at scientific researches.

In Japan, a model testing machine of a large isotope separator of Smythe type magnet was constructed in Osaka University (**1**) and has been in operation since 1953, and a machine of beam radius of 80 cm was constructed in 1955 at the Institute of Scientific Research in Tokyo (**2**), and now in the Institute for Nuclear Study of Tokyo University a comparatively large machine is under construction.

At Kyoto University, the construction of a medium size isotope separator began in 1955 and was finished in autumn, 1956 (**3**). Later, the test operation of the apparatus was done and some separated isotopes have been obtained in appreciable amount by this apparatus. In the following sections, the outlines of the isotope separator in Kyoto University are described, and some detailed data obtained in its operation are discussed.

2. Outlines of isotope separator

The main specifications of European isotope separators as compared with Kyoto-Separator are listed in Table 1. This apparatus is composed of a main magnet, an ion deflection chamber, a low voltage arc type ion source, and an ion collector. These

Table 1.

Situation	Year of completion	Type of magnet (deflection angle)	Magnetic gap (cm)	Radius of the magnet (cm)	Weight of magnet (ton)	Maximum magnetic field (gauss)	Maximum acceleration voltage (KV)	Literature
Copenhagen	1941	90°	6.0	80	4.5	8,000	70	**4**
Stockholm	1948	90°	10.3	160	6.5	3,500	60	**5**
Amsterdam	1952	180°	17.0	100	40	3,150	25	**6**
Saclay	1952	60°	6.6	50	5	12,000	35	**7, 8**
Kyoto	1956	60°	8.0	60	7	8,000	50	**3**

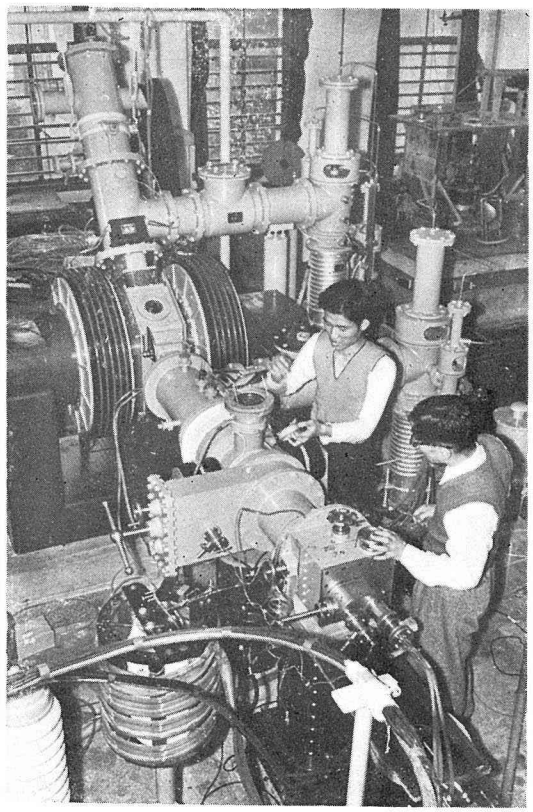

Fig. 1. Photographic view of isotope separator in Kyoto University.

main parts of the apparatus, as well as vacuum system and driving electric circuits, are described in the following sections. The main features of this apparatus are illustrated in photographic view of Fig. 1, and the vertical sectional view of the main body is shown in Fig. 2.

The magnet

The shape of the magnet pole face is pentagonal, the distance between the pole pieces being 8.0 cm, and their maximum usable width is 22 cm (edge length=40 cm). This usable width can be varied by the movable wing shutter, so that the half diverging angle of the ion beam entering the magnetic region from the ion source is varied from zero to the maximum of 6° (~0.1 radian). The ion optical relations of ion beams

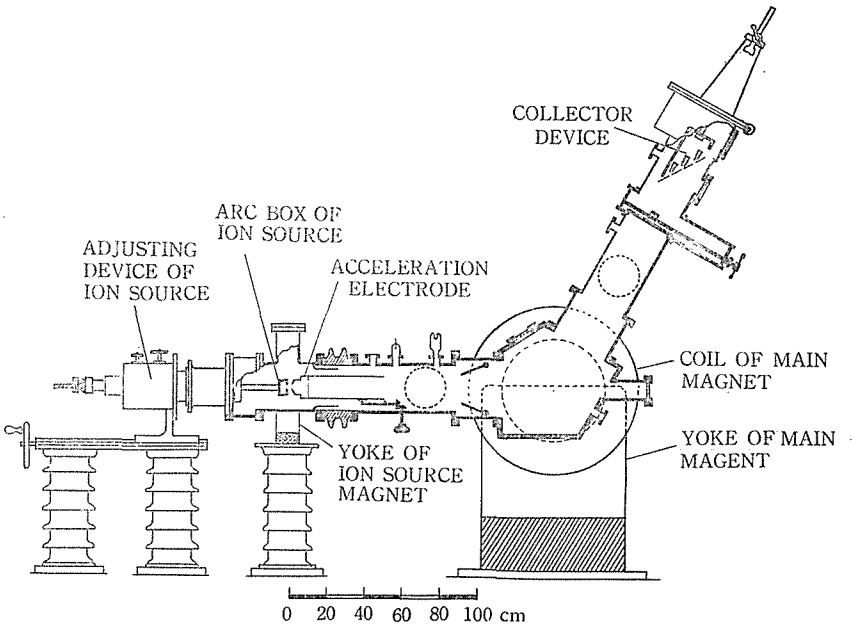

Fig. 2. The vertical sectional view of the main body of the separator.

are illustrated in Fig. 3. As is well known, the mass dispersion D and the second order aberration B in the symmetric arrangement of 60° wedge type magnet are represented as follows:

$$D = r_0,$$

$$B = \alpha^2 r_0,$$

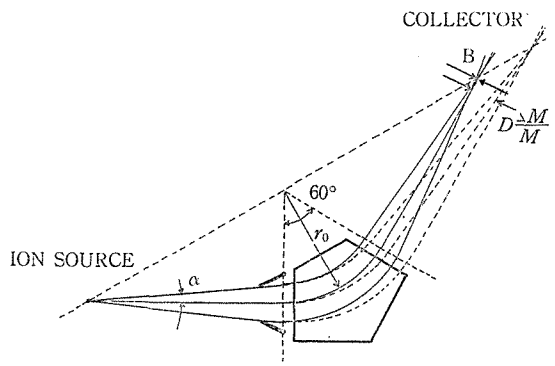

Fig. 3. Ion optical relation in the separator.

where r_0 is the radius of curvature of ion beam and α is the half diverging angle of primary ions. In this apparatus $r_0 = 60$ cm, and so the distance between the ion beams of atomic mass number A and $A+1$ at the focal point is represented by

$$D\frac{1}{A} = \frac{r_0}{A} = \frac{60}{A} \text{ cm.}$$

Therefore the image displacement for one atomic mass number difference at $A=200$ (mercury ions) is 3 mm. On the other hand, the width of the image is represented by

$B+$(width of the slit of ion source).

Thus if the slit width is 2 mm, α is permitted to be 0.04 radian ($\sim$2.3°), for the separation of neighbouring isotopes of mercury. These values show that the machine is capable of separating the isotopes of almost all elements. However, these values are for ideal cases, and in practice they are considerably affected by many factors; namely (1) stability of ion acceleration voltage, (2) homogeneity and stability of magnetic field strength, (3) scattering of ion beams by residual gases, and (4) broadening effect of space charge on the path of ion beams.

Because of the so-called fringing effect of the magnetic field boundaries, the actual magnetic pole boundaries were retired by 9 cm from the ion optical boundaries.

The configuration of magnet yoke (Figs. 1 and 2) is of *C* type, and its gap is vertical. The iron of the magnet is a low carbon steel (carbon content being less than 0.06%). Two exciting coils are provided and each coil consists of 6 layers of 150 turns of copper ribbons and of the cooling copper sheets soldered to the cooling pipes at the round edges (Fig. 1). Total electric resistance of two coils in series is about 3.2 ohm, and the temperature rise of the coils is 25°C after loading the current of 37.5A for 5 hours at room temperature of 16°C and with the circulating rate of cooling water of 32 litre/min. The magnetic field strength at the centre of the magnetic gap is measured and the excitation curve is illustrated in Fig. 4.

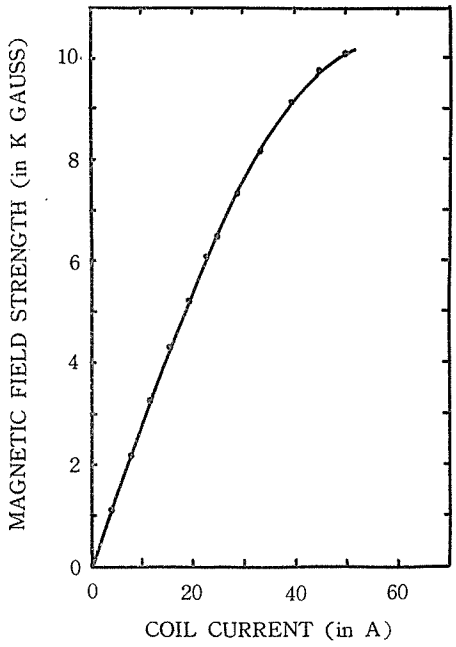

Fig. 4. Excitation curve of the magnet.

Deflecting vacuum chamber

The vacuum chamber is a pentagonal rigid box constructed with two parallel iron walls of 8 cm thickness, and five side walls of brass. The iron walls serve as the magnetic pole pieces by fixing the chamber between the magnetic yokes. The mechanical accuracy and strength of the chamber is maintained by the five spacers at the corners as well as the five side walls fixed to the iron walls. On the other hand, the vacuum seal is achieved by soldering the edges of thin copper sheets which are also soldered to the boundary edges of each iron walls and brass side walls by hard solder. The mechanical error of the magnetic gap distance is $\pm$3.5/100 mm over the

whole pole face, so that the homogeneity of the magnetic gap distance is within the error of 0.05%. On the inner surface of the chamber, thin exchangeable linings of copper sheets are provided for the protection from the erosive effect of various material ions.

Vacuum system

Two sets of evacuating pumps are employed. Each set of pumps consists of an 8 inch oil diffusion pump with the pumping speed of 1250 litre/sec at 2×10^{-6} mmHg and a Kinney type rotary pump with pumping speed of 680 litre/min at 1 mmHg. Arrangement of the vacuum pumps and many valves are schematically illustrated in Fig. 5. Some of these valves are operated by the compressed air supplied through the electromagnetic valves from a 4 atm. air compressor, and these valves can automatically shut down the pumping system for the protection of the apparatus under various accidents, namely the stopping of the cooling water and electrical power supply, or the sudden leakage in the vacuum system.

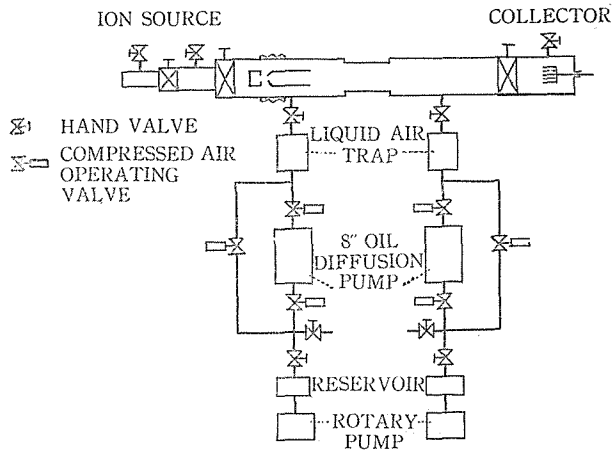

Fig. 5. Vacuum system of the isotope separtaor.

The exchanges of the filament of ion source, the whole assembly of ion source and the ion collecting devices may be done, keeping the vacuum of the main parts of the apparatus. The adjustments in all directions and slight rotations of ion source position are possible without affecting the vacuum.

Ion source

Structure of the ion source used for gaseous samples are illustrated in Fig. 6. A carbon box placed between the magnetic pole tip is the arc chamber. Electrons emitted from the wolfram filament

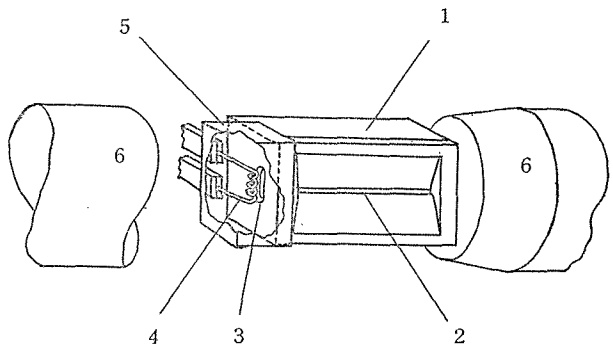

Fig. 6. Ion source for gaseous samples
1. arc box (carbon) 2. slit 3. discharge slot
4. filament 5. filament cover
6. pole of magnet

enter through the discharge slot (4 mm×8 mm) of the side wall of the box along the magnetic field direction, and the plasma column of arc is produced behind the narrow slit (1～2 mm×50 mm) of the front wall of the arc box. The sample in gaseous state is introduced into the arc box through a pipe with a gas leak adjuster outside the apparatus.

For solid state samples, the crucible of alumina heated by the molybdenum wire is furnished under the arc box (Fig. 7). The sample in the crucible is evaporated at an appropriate temperature maintained by the automatic controller with thermocouple temperature guage. Evaporated gas of the sample is led to the position of arc column by the defining chimney of stainless steel.

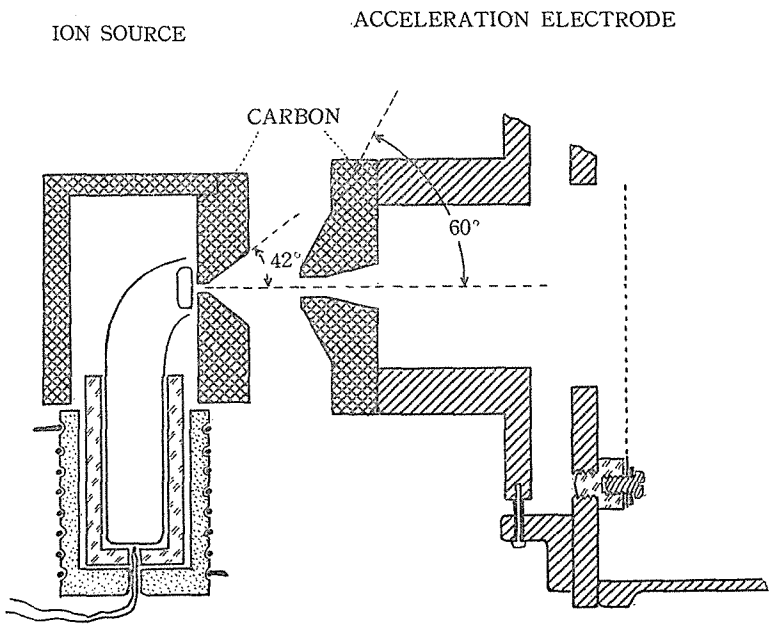

Fig. 7. Ion source for solid state samples and acceleration electrode.

The wolfram filament (1 mm dia.) of 6 turn spiral (outer diameter=4 mm) is heated by direct current of maximum 50A and is maintained at the negative potential of maximum 300 volts with respect to the potential of the arc box. The repeller electrode plate of stainless steel placed at the position opposite to the electron introducing slot is insulated from the arc box, so that the potential of this electrode is negative as the result of the accumulation of electron charges, and thus it serves to increase the ionization efficiency by the electron reflection.

The whole system of the ion source is in the positive potential (maximum 60 KV), and the extraction of ions as well as the acceleration of them are carried out by an acceleration electrode in the ground potential. This cylindrical electrode of stainless

steel has a bill of carbon at the end faced to the ion source slit, and the length of acceleration gap (Fig. 7) is finely adjustable by a screw outside the apparatus. In the cylinder of acceleration electrode, a grid of molybdenum fine mesh is spread near the carbon bill, and is electrically insulated from the electrode so as to supply negative potential of several hundred volts for the use of space charge compensation.

Stabilization of magnetic field

The magnet coil current is delivered by a 10 KW motor generator and is stabilized by a high current regulator (**9**). The schematic circuit of this regulating system is illustrated in Fig. 8. Total magnet current gives a voltage drop over the 40 mΩ manganin resistance series to the main coil circuit. The difference between this voltage

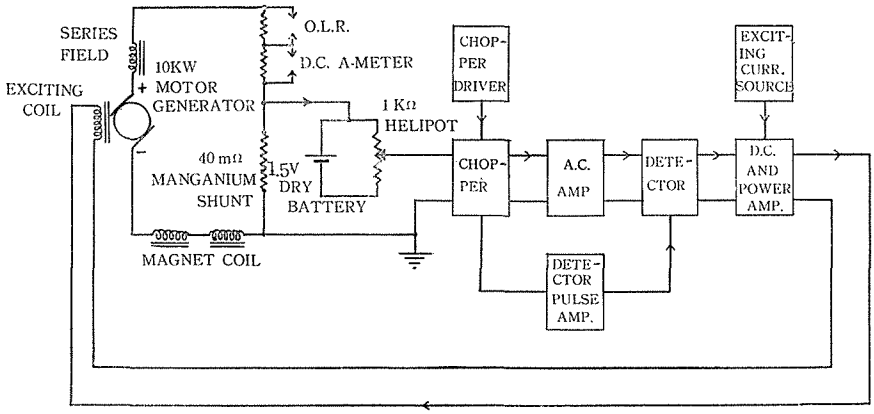

Fig. 8. Magnet current stabilizer.

and the voltage of a standard battery is amplified by the system of a 400 cycle chopper-converter, an a. c. amplifier, a phase detector, and a d. c. amplifier, whose output voltage controls the grid of valve 807 output power stage. The output current from the cathode of the valve 807 is fed back to the field coil of main d. c. current generator.

The stability of this current supplying system was measured to be within the deviation of 1/4000 at the current of 10A during 3 hours continuous operation.

Stabilization of acceleration voltage

Acceleration voltage is supplied by a d. c. high voltage source of rectifier-condenser system, and is regulated (**10**) by the valve 5T31 (Fig. 9). Divided voltage derived from a carbon resistor is referred to the voltage of standard dry cells (67.5 V, 135 V, or 202.5 V), and the difference of these voltages is amplified and this modulates the 4 MC high frequency oscillation. By a well-insulated high frequency transformer, the modulated high frequency oscillation supplies the control voltage through a rectifier

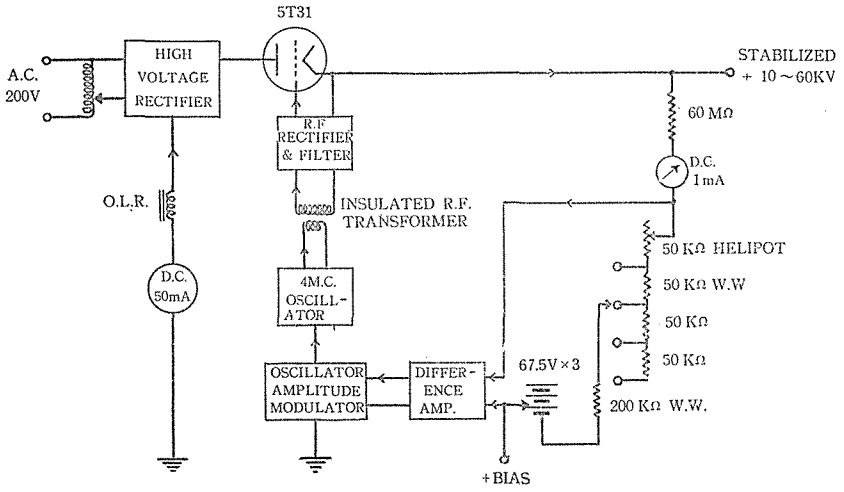

Fig. 9. Acceleration voltage stabilizer.

unit to the grid of valve 5T31. The acceleration voltage can be adjusted precisely to any desired value by the switching of 50 KΩ resistors and by the continuous rotation of helical potentiometer at the lowest stage of dividing resistors.

The stability of this voltage supplier was measured after 30 minutes warm up period to be about 1/2000 at the voltage of 25 KV.

Collector device

The collector device consists of a framework or a plate cooled by water and the attachments of various type collecting pockets. These collecting pockets are to be made of the materials suitable for the properties of ions collected. Some materials were tested in various forms. For the magnesium ions stainless steel boxes, copper or graphite pockets were tried, and for the neon ions silver plates were used.

The whole assembly of collector devices is movable along the beam direction and may be set easily at the desired position (Fig. 10).

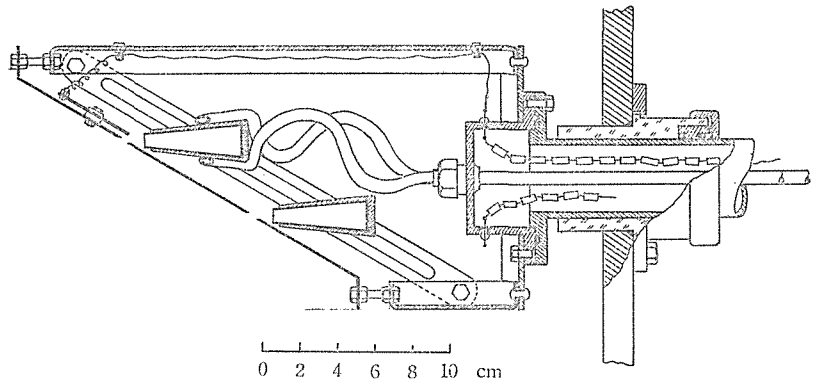

Fig. 10. Collector device.

3. Performance of the separator and discussion

The following three properties are essentially required for the isotope separator, that is

(1) collected ion current is as high as possible;

(2) the resolving power is as large as possible;

(3) the operation of the apparatus is as stable as possible during a long period.

In a primary test operation with argon, neon, or magnesium ions, we could not obtain satisfactory results in these respects, so various improvements and adjustments have been done. The knowledges obtained in this procedure will be discussed in the following.

Increasing of ion source efficiency

In order to obtain high collector current, it is important to have as high ionization efficiency as possible. Efficiency of the ion source is indicated by the minimum pressure of gas necessary to ignite the arc, so the factors deciding the minimum operating pressure in the ion source were considered.

In igniting the arc, it is considered that the surface of the electron emitting filament is surrounded by the double layer of ions and electrons (**11**). From this idea follows the relation:

$$J_e \leqq \gamma \sqrt{\frac{m_+}{m_e}} J_+ ,$$

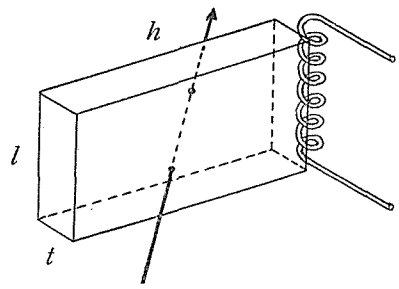

Fig. 11. Arc column.

where J_e and J_+ are the currents of electron and ion, m_e and m_+ the masses of electron and ion respectively, and γ is a correction factor of $\frac{1}{3}\sim\frac{2}{3}$.

On the other hand, the following relations hold independently, for an arc column of flat type (Fig. 11):

$$J_+ = \frac{N_0 V_n A'}{2} f_k P(j_e) ,$$

$$J_e = A j_e ,$$

where N_0: density of neutral molecule,

V_n: velocity of neutral molecule,

j_e: current density of electron,

$A=lt$: cross sectional area of arc column (area of electron entrance slot),

$A'=lh$: area of side surface of arc column,

$P(j_e)$: mean probability that a neutral molecule is ionized in its passage through the arc column,

f_k: ratio of the number of ions reaching the filament to the total number of ions produced by ionization.

The function $P(j_e)$ depends on V_n as well as on the shape of arc column, and for small values of j_e it is nearly proportional to j_e.

From the above three relations it is derived that

$$N_0 \geq \frac{2}{r\sqrt{V_n}}\sqrt{\frac{m_e}{m_+}}\,\frac{1}{P_0(j_e)}\,\frac{1}{hf_k},$$

where $P(j_e)=tj_eP_0(j_e)$.

According to this relation it is evident that $P_0(j_e)$ and f_k must be increased to decrease the minimum value of N_0. To increase f_k, we made some improvements over the area, form, and depth of electron entrance discharge slot, and adjusted the filament position to the discharge slot. To increase $P_0(j_e)$ we furnished the floating type repeller electrode for electron reflection (8), and made some adjustment of the chamber position relative to the source magnet. Moreover we increased the number of turns of the filament spiral, and covered the filament part outside the arc box to increase the density of neutral molecule near the filament. In the case of solid sample, e. g. magnesium, we also employed a vapour confining chimney of stainless steel (8) in the graphite arc box as a reflector of neutral atoms and radiation. After these reformations the efficiency of the ion source appeared to be remarkably improved.

In Table 2, the achieved performances under normal operation of the ion source are listed and compared with those obtained before.

In the case of magnesium, a remarkable improvement was readily seen by the fact that the glass of the peep window of the ion source parts which had been silvered by the vapour of neutral metallic magnesium in a minute after igniting the arc, remained almost un-silvered during several hours' operation.

Table 2.

Operating conditions of ion source	Argon		Magnesium	
	before	now	before	now
Gas supply (cc N.T.P./hour)	250	50		
Arc discharge current (A)	0.5	0.5~1	0.2	0.2~0.8
Applicable voltage of acceleration without spark down (KV)	10	30	15	30
Collector current (mA) (no correction for secondary electron emission at the collector, $2\alpha=12°$)	0.2	3	0.2	5

The relation between the acceleration voltage and the collector current is shown in Fig. 12, for various values of acceleration current. The acceleration current is a total load current of the high tension set, which includes total ion current extracted from the ion source, and the small contribution of electron current to the ion source. The value of this acceleration current is nearly constant with the increase of extraction voltage, because the current value is determined mainly by the ion density of the ion emitting plasma surface and its area. It is readily seen in Fig. 12 that at the lower acceleration voltage the collector current is poor. This is due to the space charge divergence of the beam at the accelerating gap at lower voltage, and will be improved by the more refined focusing property of the accelerating electrode system. With the electrode system of this apparatus 30 KV is needed for mA-order operation, and this voltage value is somewhat higher than the theoretically (Pierce's geometry (**12**)) expected one.

In conclusion, the improvement of ion source efficiency lead to the reduction of

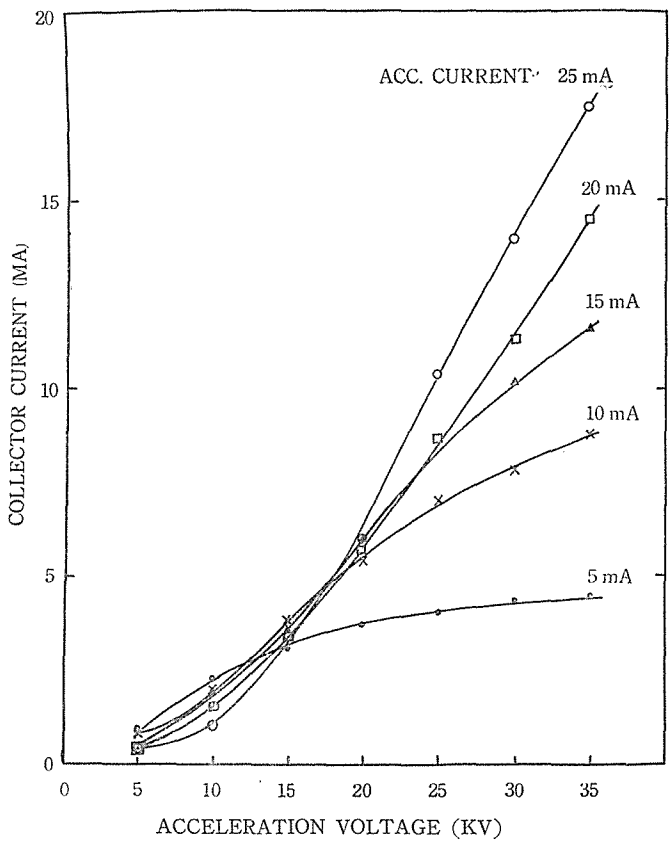

Fig. 12. Relation between the acceleration voltage and the collector current.

gas supply, and accordingly permitted the application of high accelerating voltage without spark down, and decreased the loss of ions scattered by the residual gas, and then resulted the increases of ion current reaching the collector.

The resolving power and the affecting factors on it

The breadth of the ion beam at the collector is largely affected by the deviation of focal point, and the minimum beam width obtainable at the focal point is determined by many factors; namely, the space charge broadening effect, scattering of the ion beam by the residual gas, ion optical second order aberration and object width, fringing fields effect, inhomogeneity of the initial velocity of ions, and the local inhomogeneity of magnetic field strength. Of these, the last two are estimated to be very small. Because the measured ripple voltage of the acceleration at 30 KV is about 10 V peak to peak, and considering that in the low vlotage arc type ion source no appreciable voltage gradient exists, initial velocity inhomogeneity is less than 1/1000. The local magnetic field inhomogeneity has not been measured but must be

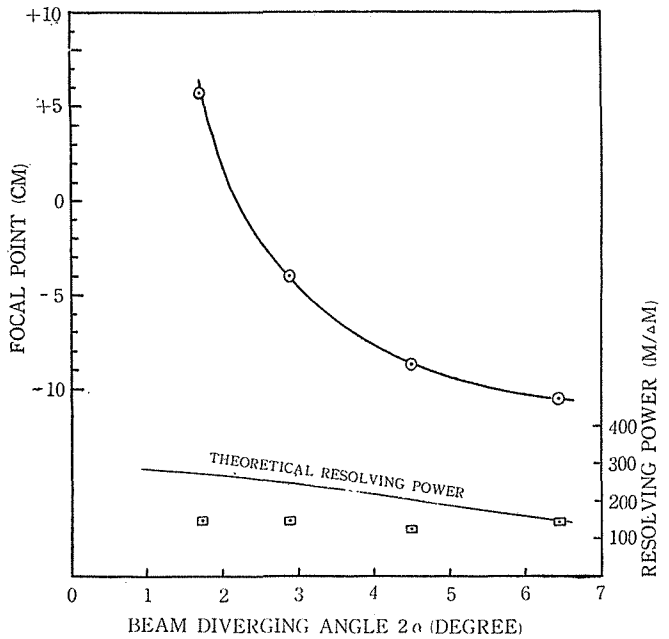

Fig. 13. Variation of focal point (⊙) as a function of beam diverging angle 2α. The origin of the ordinate is the expected focal point (Fig. 16), and positive sign means the direction opposite to the deflection magnet. Limit of error in focal point determination is about ± 2 cm. Beam resolving power obtained at each angle is also shown (⊡). Theorteical resolving power was calculated considering the object width to be that of ion source slit, 2 mm. These data were obtained by the use of the Mg^{24} ion beam accelerated to 26 KV, and the collector current was 4.5 mA at $2\alpha=6.4°$.

small considering the mechanical accuracy of the length of magnetic pole gap $\left(\pm\frac{3.5}{100}\text{ mm}\right)$. So, in the following, we will discuss the other factors.

To determine the true focal point, a Faraday cage with a slit of 1.5 mm width and 40 mm length was mounted on a movable collector plate, and the ion beams were scanned electrically by a motor driven helipot. The output current from the Faraday cage was recorded on an electronic recorder chart. The spectrum of the images was thus measured at the various positions along the central axis of the collector side arm, and the base width of the beam as well as the variation of spectrum shape were taken as a measure for determining the focal point.

The focal point thus determined was found to vary considerably with the beam diverging angle, ion current intensity, or ion source conditions. Fig. 13 shows the observed variation of focal point with the diverging angle 2α. Fig. 14 shows the variation of it with ion current intensity. Beam resolving power observed (calculated from the width at $\frac{1}{10}$ of the maximum) is also shown in each case. Other parameters such as vacuum condition and acceleration voltage were noticed to affect the focusing

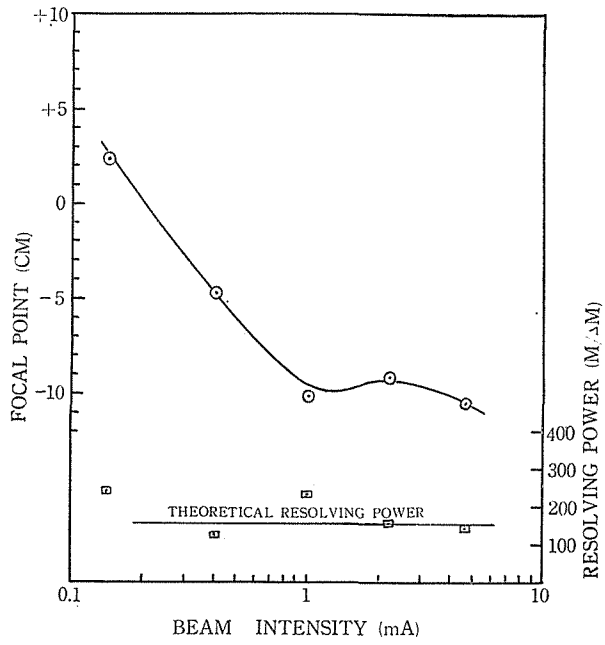

Fig. 14. Variation of focal point as a function of beam intensity. Coordinate of focal point is taken as in Fig. 13. Limit of error in focal point determination is ± 2 cm. Beam resolving power obtained is also shown. Mg^{24} ion beam was used and beam diverging angle 2α was 6.4°, acceleration voltage being 25 KV.

property in smaller extent, but the exact relations were not examined.

Theoretically, if the ion beam of the intensity of 1 mA/cm or more were not neutralized at all, it would diverge outside at the exit boundary of the magnetic field by its own space charge, and would have electric field of about 100 volts/cm at the surface (Fig. 15). In practice, however, beam absorbs electrons created by the ionization of the residual gas, making itself a kind of plasma. An imperfectly neutralized part of the beam, however, produces electric field in the beam. This field makes the trajectory of the charged particle parabolic, and leads to the focal point displacement (Fig. 16). By the two-dimensional calculation of the path of ion beam, postulating the beam intensity to be equal to any direction, focal point displacement Δf is obtained to be

$$\Delta f = \frac{5E_s}{2V\alpha} r_0^2,$$

where E_s is the electric field at the beam surface and V is the acceleration voltage. E_s indicates the degree of neutralization and is determined by the rate of production and loss of slow electrons. E_s is not considered to depend on α markedly, and so the above relation explains the $1/\alpha$ dependence of Δf as observed in Fig. 13.

Beam intensity modulation due to plasma oscillation with a frequency of about 15~50 KC was observed, which makes the space charge neutralization incomplete, and results in the increase of E_s. The ratio of the amplitude of this high frequency current to the time averaged total current changed with the ion source conditions as is shown in Fig. 17. This will explain the focal point variation as shown in Fig. 14.

The focal point displacement caused by the variation of virtual object point was estimated to be maximum +2 cm~−5 cm. This may also account for a part of the observed one.

From the above expression of Δf and Fig. 13, we can conclude that if no space charge effect existed, the ion optical focal point is deviated by (-16 ± 2)cm from the expected one. This means 2 cm over correction of the magnet boundary (9 cm correction was made for 8 cm gap length), although focal point displacement Δf, due to space charge, partly compensates this circumstance. These relations are presented in Fig. 16.

Beam scattering due to residual gas was found to be appreciable at the pressure above $\sim5\times10^{-5}$mmHg, especially in the case of rare gas ions or heavy ions. On the other hand, below $\sim2\times10^{-6}$mmHg, space charge compensation became insufficient, and considerable broadening was observed with the Mg^+ beam of a few mA intensity. But around 1×10^{-5}mmHg, beam width *versus* pressure relation was rather flat, although these absolute pressure values would vary somewhat with the nature of the ions and the residual gases.

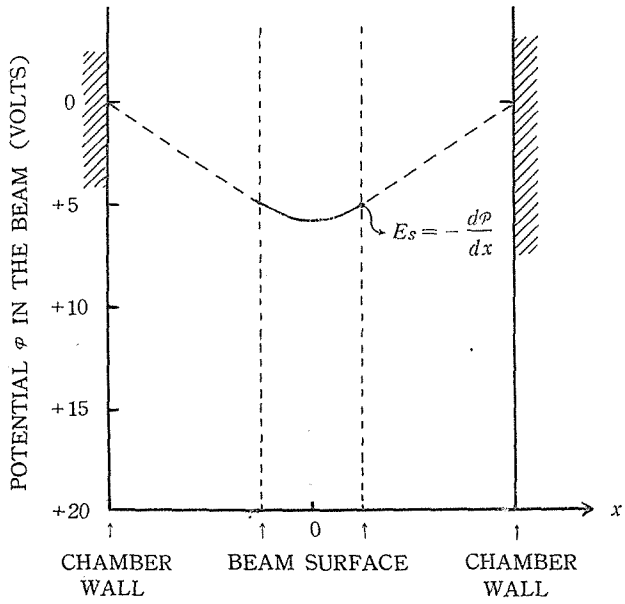

Fig. 15. Potential distribution inside and outside the beam. Potential value at the valley varies according to the degree of neutralization.

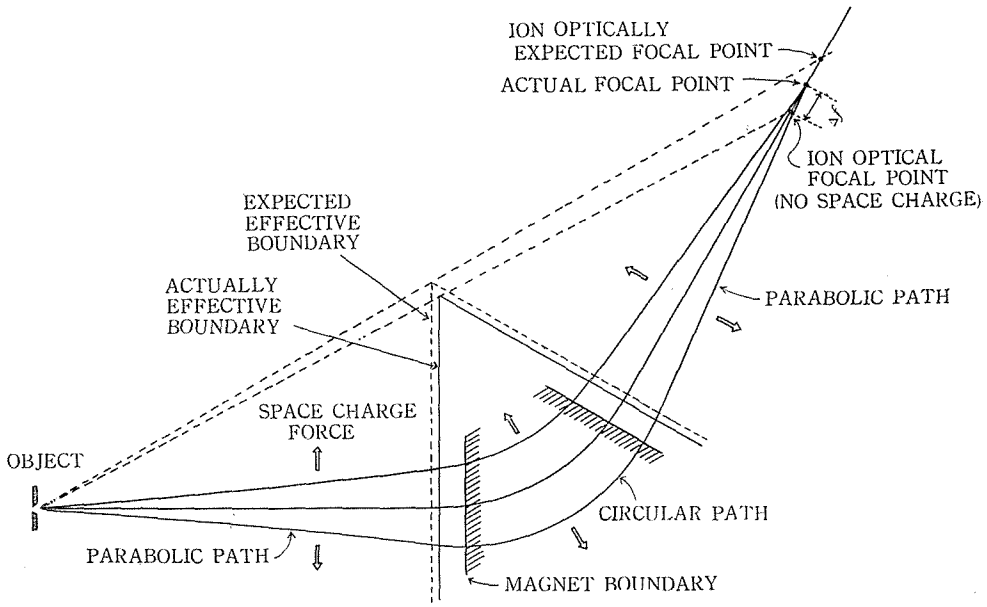

Fig. 16. Focal point displacement due to space charge effect.

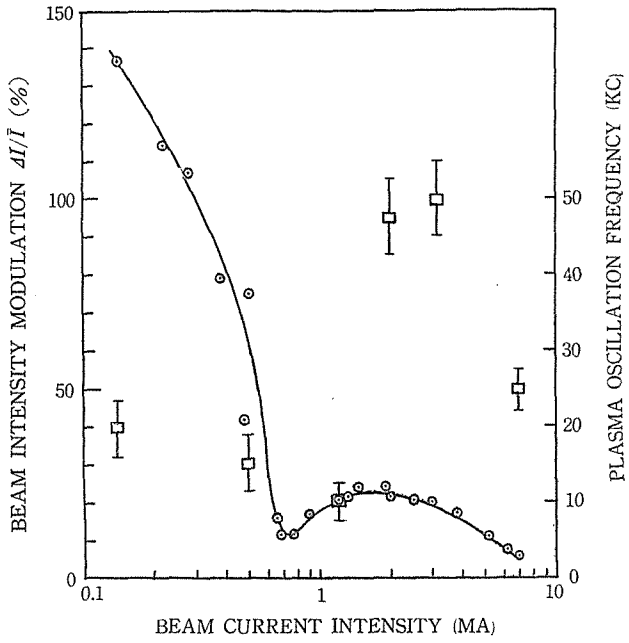

Fig. 17. Observed relation of beam intensity modulation to beam current intensity. The points ⊙ show the modulation ratio $\Delta I/\bar{I}$, and the points □ show the oscillation frequency. ΔI is a peak amplitude of modulation and $\bar{I}$ is a time average value of beam current.

Stray magnetic field of a few hundred gauss due to ion source magnet exists behind the accelerating electrode as well as between the accelerating gap. It is troublesome because the ion beam receives slight deflection in passing through this region, resulting the deflection of beam centre axis of several degrees in light element ions. This deflection can be corrected to some extent by adjusting the position of ion source chamber relative to the accelerating electrode, though this procedure sometimes results in broadening the object width. In view of space charge compensation, however, this stray field may play as stopping action for the flow of slow electrons, which in case of no magnetic field flow back to the ion source along the potential gradient in the beam, and makes space charge compensation insufficient.

In order to stop the flow of slow electrons to the ion source, a grid of fine molybdenum mesh with a potential of maximum −350 volts was mounted behind the acceleration electrode according to Bernas (8), but it showed no improvement upon the minimum beam width at the focal point. So the electron flow is considered to be already prevented from escaping by other effects such as stray magnetic field mentioned above, and we dismounted the grid.

Curving of beam image at the collector plate mounted normal to the beam direc-

tion was observed, which is mainly due to fringing fields effect. Radius of curvature of the image was (80±5)cm compared to the theoretical value (**13**) of (250±100)cm calculated with the geometry of this apparatus. This discrepancy suggests other effects than purely two-dimensional fringing fields effect. Anyway, image curvature is almost negligible for practical purpose.

In conclusion, we may say that in spite of the complexity of beam focusing property owing to the space charge and other effects, appropriate adjustment of the collector position makes $M/\Delta M \sim 150$ attainable in normal operation, and $M/\Delta M \sim 250$ in favourable conditions as can be seen in Figs. 13 and 14.

4. Actual performance of the isotope separation of several elements

In general, charged materials in the arc box of the ion source must be in gas phase. In this point, almost all the elements are classified into three groups in preparing for the ion source. The elements of the first group have the sufficient vapour pressure to introduce into the arc box at room temperature; for example, neon, nitrogen, argon, etc. The second is the group of the elements which can have the necessary vapour pressure (10^{-2}mmHg) at the temperature of several hundred degrees centigrade; for example, magnesium, potassium, calcium, zinc, mercury and so on. The third group contains the elements the vapour pressure of which does not reach the sufficient value at the above-mentioned temperature. In many cases the elements of the last group are charged in the forms of suitable chemical compounds, such as chloride, bromide or iodide (**14**).

We tried to separate three elements; neon, magnesium and silicon, each of which is considered to belong to one of the three groups.

Separation of magnesium isotopes

A piece of metallic magnesium was charged in the crucible of alumina which was hung under the arc box of ion source and heated by the molybdenum wire. The temperature of the crucible can be regulated by the temperature regulator with a mercury switch operated by the output voltage of a thermocouple and maintained at a constant temperature of ~300°C. On account of temperature gradient which exists between the sample and the thermocouple junction this temperature is lower than the true temperature of magnesium sample itself.

An example of the operating conditions of the separator is shown in Table 3, and an example of mass spectrum of magnesium, obtained by the separator using a Faraday cage with a slit of 5 mm width (electric scanning) is illustrated in Fig. 18.

As the collector, stainless steel boxes, copper and graphite pockets were tried. In the case of stainless steel boxes, the films of metallic magnesium accumulated on

Table 3. Operating conditions of separator in the cases of three elements.

	Magnesium	Neon	Silicon ($SiCl_4$)
Acceleration voltage (KV)	30	30.7	31
Acceleration current (mA)	8	2.5	8
Total collector current* (mA)	5	1.3	0.75
Arc voltage (V)	40	300	120
Arc current (A)	0.2	0.3	1.6
Filament current (A)	42	48.5	47
Gas supply (cc N.T.P./hour)		210	10
Ion source efficiency** (%)	5.1	1	18†
Mean pressure*** (mmHg)	5×10^{-6}	3×10^{-5}	1.1×10^{-4}
Collection hour (hour)	3	4	$3\frac{1}{4}$

* At $2\alpha=6.4°$.
** Ion source efficiency is the ratio of the number of ions extracted from the ion source to the number of neutral atoms consumed in the ion source.
† Percentage of Si^+ is assumed to be 27%.
*** Reading of ionization gauge calibrated for air.

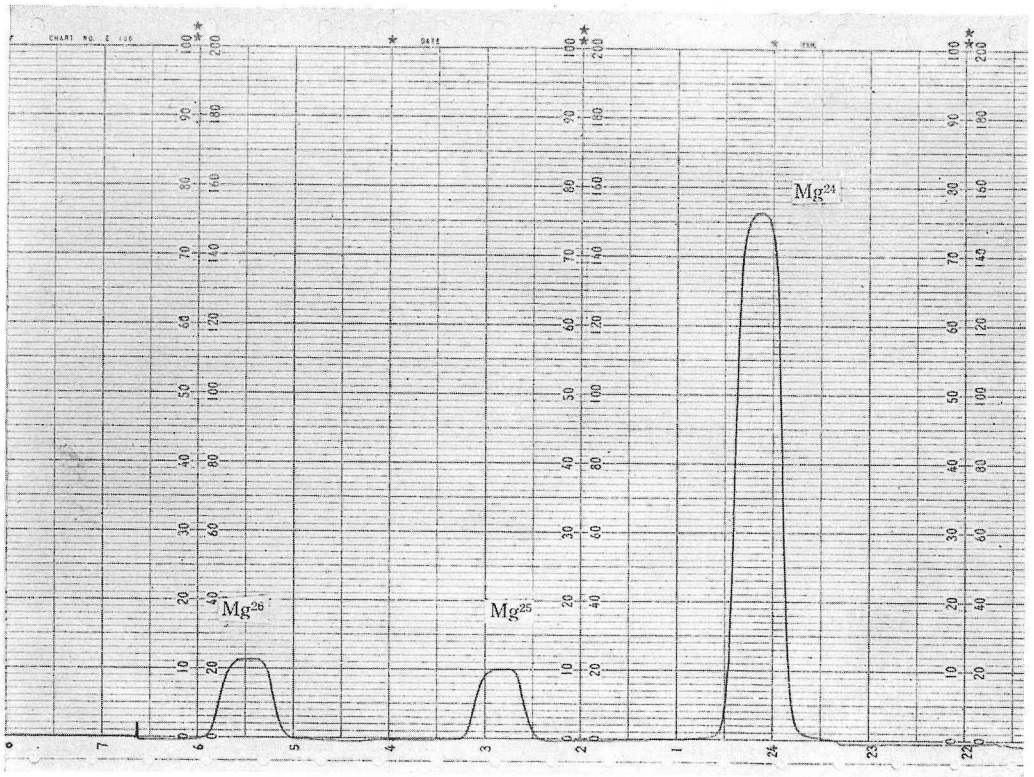

Fig. 18. Mass spectrum of natural magnesium. 5 mm slit Faraday cage was used as an ion collector.

the backward surface of the box unexposed to the direct ion beam easily exfoliated from the surface. On the surface directly exposed to the ion beam no accumulation was recognized. In the case of copper pockets, however, the metal films on it tightly held like the electroplating, and the accumulated amount of magnesium at the positions of direct bombardments was about 150μg/cm^2 per hour.

For the ion current over $\sim$200μA/cm^2, re-sputtering to the neighbouring walls increases appreciably, and almost no accumulation is recognized at the directly bombarded positions. In the case of graphite collector the re-supttering phenomenon is weaker so that the efficiency of direct deposition is better than in the case of copper collector.

Separation of neon isotopes

The collection of ions of gas samples, especially chemically inactive noble gases, is achieved by the method of ion bombarding. This method was tried by Koch (**4**, **15**) and by other authors (**16**, **17**), and the calculations about the range of 50 kev ions in metal are presented by Nielsen (**18**).

We have applied this method to the collection of neon isotopes. The apparatus of gas supply is shown in Fig. 19, and an example of the operating conditions of the separator is listed in Table 3.

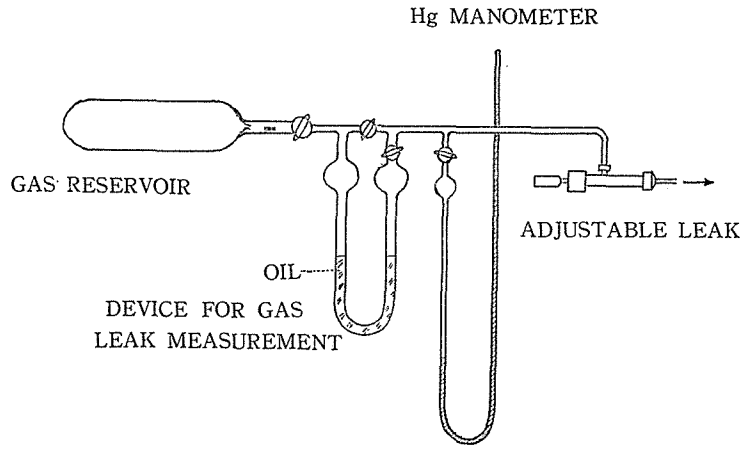

Fig. 19. Apparatus for gas supply.

As the collector material, the silver plates were used. The thin silver plates of 1.3 cm$\times$10 cm$\times$0.02 cm were polished and heated red hot in the induction vacuum furnace for about two hours and the absorbed gas in silver was driven out. Then these degassed silver plates were mounted tightly on the collector plate of the isotope separator and bombarded by the 30 kev ion beams of separated neon isotopes 20, 21 and 22 for 1.5$\sim$4 hours with 3$\sim$10μA/cm^2 intensity. Irradiated plates were removed

and again heated in the quartz tube induction vacuum furnace to the temperature slightly lower than before for a few minutes, and the gas evolved from the silver was collected in a vessel of the volume of 108 cc. The apparatus used in these gas processings is shown in Fig. 20. The mass analysis of these collected gas samples were performed by the C.E.C. Model 21-401 mass spectrometer*. An example of these mass-spectroscopic patterns (after correction for the background and for time variation of the pressure in sample gas container) is illustrated in Fig. 21. From these mass pattern the relative quantities of three neon isotopes in each isotopically separated sample were calculated with the correction of A^{++} and CO_2^{++} contributions and are listed in Table 4 together with their collection conditions. The quantities of impurity gases mainly caused by the absorption of air were relatively so large that the values of the isotopic purities of the separated neon were not very accurate. The quantities of separated neon which was held in the collector silver plates were calculated from the sensitivity of the spectrometer and the spectrum peak height. The quantities of neon caught and held in the thin layer of metal surface cannot be increased proportionally to the increase of integrated current of bombardment,

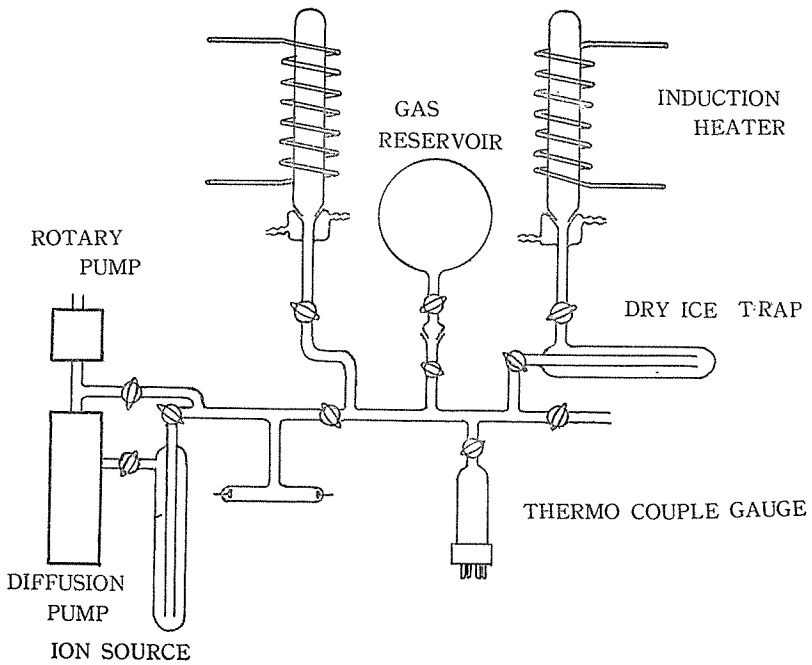

Fig. 20. Apparatus for gas preparation.

* This mass spectroscopic analysis was carried out by Mr. T. Makita in Sasaki Laboratory in the Department of Chemistry in Kyoto University.

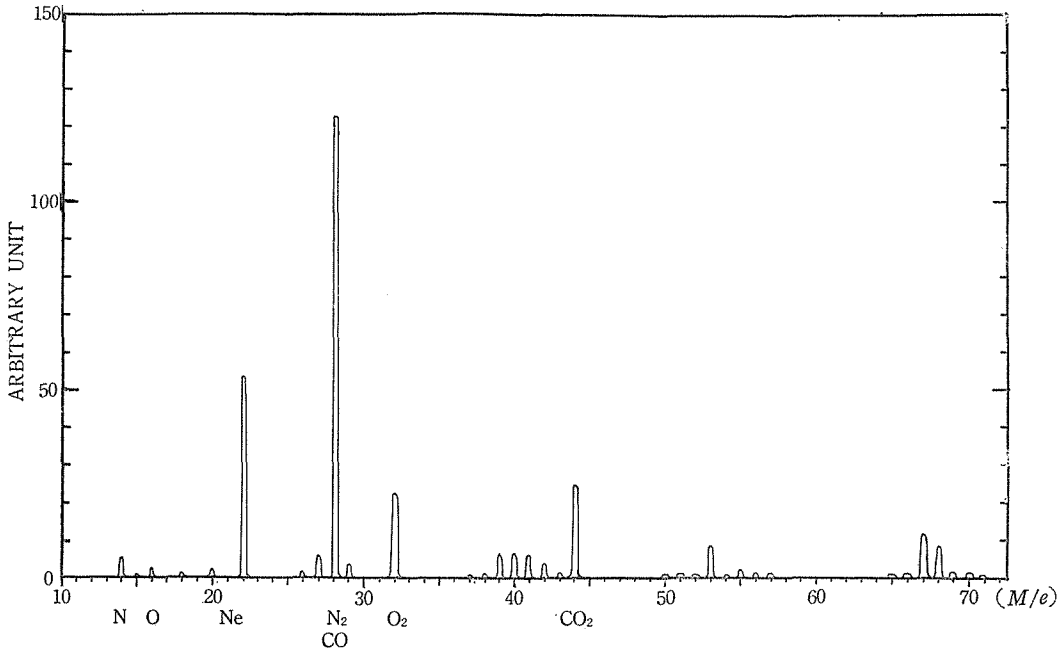

Fig. 21. Mass spectrum of sample No. 5. (enriched in Ne^{22}). Each peak value is corrected for time variation of sample gas pressure and background of the spectrometer.

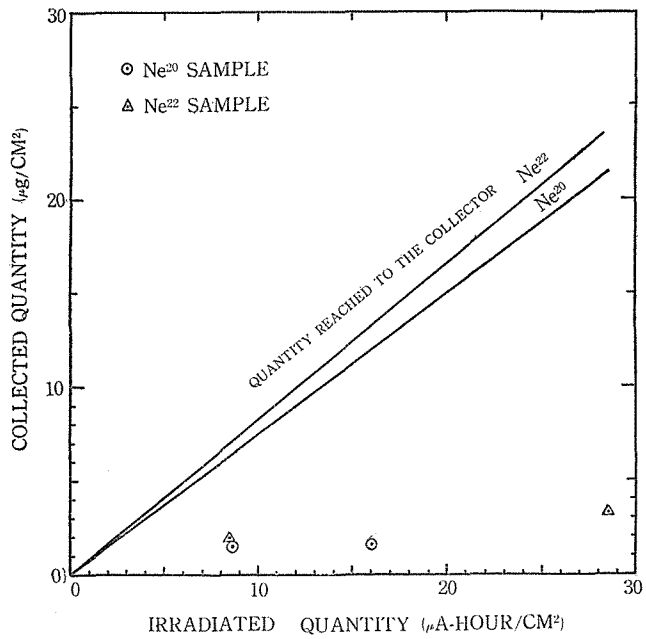

Fig. 22. Collected quantity is shown as a function of irradiated quantity. Saturation phenomenon is clear.

Table 4.

Sample number	Collected isotope	Current density ($\mu A/cm^2$)	Collection time (hour)	Irradiated area (cm^2)	Collected quantity ($\mu g/cm^2$)	Collection efficiency (%)	Isotopic purity (%)**		
							Ne^{20}	Ne^{21}	Ne^{22}
1	Ne^{20}	10.7	1.5	1.9	1.6	14	100±3.5	0.0±0.4	0.0±2.0
2	Ne^{20}	3.4	2.5	5.5	1.6	25	$99.2\ ^{+0.9}_{-1.8}$	$0.0\ ^{+0.1}_{-0.1}$	$0.8\ ^{+0.6}_{-0.7}$
3	Ne^{21}	0.88/S	4.1	S*	0.69/S	25	66.0±9.8	15.1±3.2	$18.9\ ^{+5.4}_{-7.6}$
4	Ne^{22}	3.4	2.5	0.57	2.0	28	2.3±5.6	0.0±1.2	97.7±6.8
5	Ne^{22}	7.0	4.1	4.3	3.3	14	$2.6\ ^{+1.1}_{-1.0}$	0.0±1.0	$97.4\ ^{+1.8}_{-1.5}$
natural neon***							90.92	0.257	8.82

* Irradiated area could not be measured accurately in this case, so it is designated by S.
** ± indicates the limit of error in linear scale.
*** These isotopic abundances of natural neon are the values obtained by A.O. Nier (Phys. Rev. **79** (1950), 450)

but saturate at an amount of content (as clearly seen in Fig. 22 and Table 4). In our experiment at the acceleration voltage of 30 KV, the saturated value was about $3\mu g/cm^2$ which is consistent with the value obtained by Koch (**4**) and Thulin (**17**).

Separation of silicon isotopes

Silicon is a solid state element which has the melting point of high temperature, namely 1414°C. But the silicon tetrachloride $SiCl_4$ is a liquid state compound that has the vapour pressure of 22 cmHg at 20°C. We used the vapour of silicon tetrachloride as sample, and introduced into the arc box through a leak valve as in the case of neon separation. Silicon tetrachloride and its dissociated product chlorine are both chemically very active materials, so that the special precaution is needed for the protection of pump oil, especially of the rotary pumps. For this purpose liquid air traps were used between the diffusion pumps and evacuated main body. In the preliminary tests of this chemical effect using another small rotary pump, we have experienced that if the liquid air trap was not used the oil in the rotary pump became violet coloured after about 14 hours pumping of the total of 160 cmHg–l of silicon tetrachloride vapour.

We observed the cracking pattern that indicated the mode of dissociation of the molecules in the arc box of ion source. An example (corresponding to the case II in Table 5) of the mass spectrum obtained by the magnetic field scanning with a deep and wide slit (5 mm×40 mm silt) Faraday cage is illustrated in Fig. 23. In this spectrum

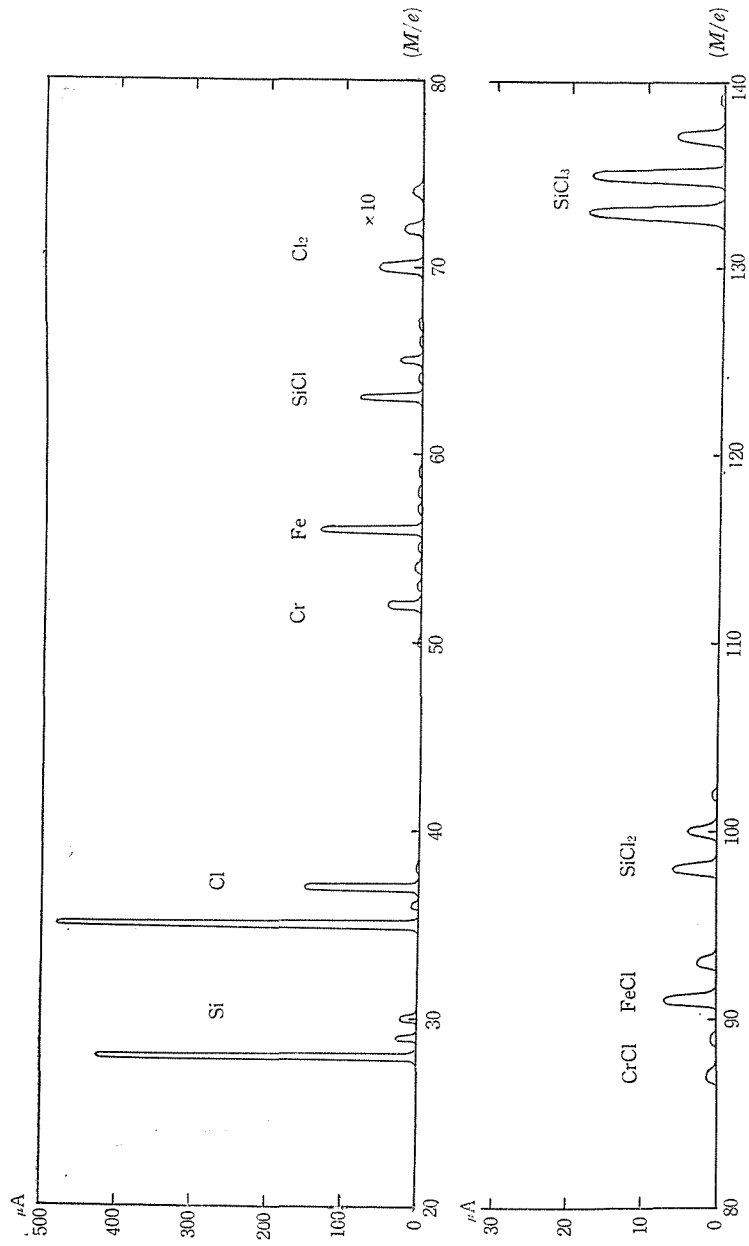

Fig. 23. Mass spectrum of $SiCl_4$ and contaminant material.

some peaks are assigned to the iron and chromium that should be originated from the stainless steel sheet in the graphite arc box. The cracking patterns of tetrachloride are influenced by the conditions in the ion source. But this dependence is very complicated and difficult to examine because the conditioning factors of the ion source cannot be stabilized in this apparatus. Also, mass discriminating effect of the ion source magnet

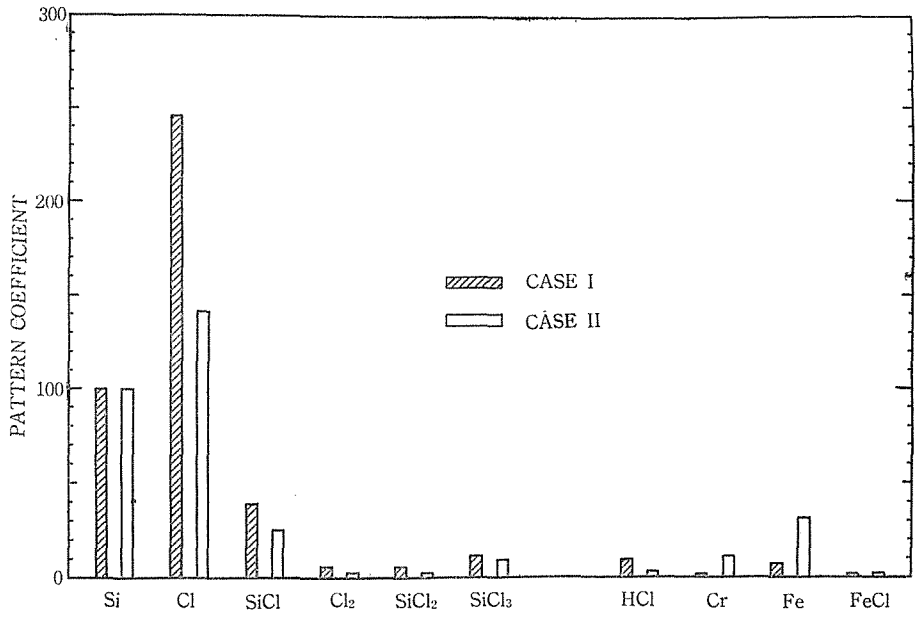

Fig 24. Cracking pattern of $SiCl_4$ and contaminant compounds. Ion source operating conditions in each case are shown in Table 5.

Table 5. Operating conditions in two cases of Si separation

		Case I	Case II
Gas supply	(cc N.T.P./hour)	6.5	13
Arc voltage	(V)	150	150
Arc current	(A)	0.9	3.0
Filament current	(A)	48	45
Acceleration voltage	(KV)	31.5	31.5
Acceleration current	(mA)	3.3	15.9
Collector current*	(mA)	0.3	1.6
Percentage of Si^+**	(%)	23.4	30.4
Ion source efficiency***	(%)	9.9	31.2
Mean pressure	(mmHg)	6×10^{-5}	1.6×10^{-4}

* At $2\alpha=6.4°$
** Percentage of Si ions in the all ions extracted from the ion source.
*** Ratio of the number of ions Si^+ extracted from the ion source to the number of neutral $SiCl_4$ molecules supplied to the ion source.

was noticeable, and wide beam collection must be employed. Pattern coefficients in two different conditions of gas supply are shown in Fig. 24, and operating conditions in these cases are listed in Table 5.

A comparison of these two indicates that the high pressure (strong arc) operation is preferable with respect to the mono-atomic ratio of cracking pattern.

The collector box is made of copper plates of 1 mm thick. The operating conditions in actual collection are described in Table 3. After these operations the separated silicon isotope Si^{28} of a few mg and Si^{29}, Si^{30} of $\sim 30\mu g/cm^2$ (calculated from the integrated current) were obtained in metallic state on the copper surface. As in the collection of magnesium, abundant isotope Si^{28} accumulated mainly on the side wing wall of the collector box rather than on the portion of direct bombarding.

5. Summary

As is mentioned in foregoing sections, the isotope separator of Kyoto University has the sufficient resolving power (150~250) for the separation of almost all elements, the good stability for long time operation, and has sufficient ion current intensity (several mA continuously) for making the isotopically pure samples for the experimental use in physical researches.

About the focusing point variation due to the space charge force acting on the ion beam, several new remarks and experimental results are presented.

Now, the several experimental researches in nuclear physics are planned by use of the separated isotopes obtained by this separator.

Acknowledgements

The writers express their thanks to Prof. K. Kimura and Prof. N. Sasaki for their kind guidance throughout the construction of this apparatus and the studies of its characters. They wish to thank to Prof. K. Ogata and Mr. J. Okano in Osaka University, Assist. Prof. M. Sakai in the Institute for Nuclear Study of Tokyo University, Dr. K. Okamoto in the Institute of Scientific Research in Tokyo, and to Assist. Prof. Y. Uemura and Mr. K. Miyake in the Chemical Institute of Kyoto University for many useful advices in making the plan of this machine. They also express their thanks to Mr. I. Kumabe, Mr. H. Takekoshi* and other laboratory members in the Department of Physics in Kyoto University for their valuable advices and assistances in constructing and testing of this machine. They wish also to thank to Mr. S. Fukunaga and Mr. K. Takamatsu of this laboratory for their helpful assistance, and to thank to Dr. T. Kambara*, Dr. S. Shima, Dr. S. Saito, Mr. Y. Ohno*, Mr. T. Tsuchimoto, Mr. M. Soneda, Mr. Y. Kondō and Mr. S. Takahashi in the Hitachi Manuf. Co. for the manufacturing of this machine.

The construction of this machine was financially supported by a grant-in-aid for scientific researches of the Ministry of Education.

---

* Now at the Atomic Energy Research Establishment of Japan.

REFERENCES

1. K. OGATA and J. OKANO, Read before the meetings of the Physical Society of Japan (1953).
2. A. SUGIMOTO and K. OKAMOTO et al., Read before the meetings of the Physical Society of Japan (1955).
3. K. KIMURA, J. MUTO, I. KUMABE, H. TAKEKOSHI, K. OKANO, H. TSUCHIMOTO, M. SONEDA and Y. KONDO, Mass Spectroscopy No. 8 (Mar. 1957), 12 (in Japanese).
4. J. KOCH, *Mass Spectroscopy in Physics Research*, N. B. S. Washington (1953).
5. I. BERGSTRÖM, S. THULIN, N. SVARTHOLM and K. SIEGBAHN, Arkiv f. Fysik, **1** (1949), 281.
6. J. KISTEMAKER and C. J. ZILVERSCHOON, *Mass Spectroscopy in Physics Research*, N. B. S. Washington (1953).
7. R. BERNAS, J. Phys. Rad., **14** (1953), 34.
8. R. BERNAS, Thèses, Faculté des Sciences de l'Université de Paris, Paris (1954).
9. J. R. WOLFF and FREEDMAN, R. S. I., **22** (1951), 736.
10. R. PEPINSKY and P. JARMOTZ, R. S. I., **19** (1948), 247.
11. A. GUTHRIE and R. K. WAKERLING, *The Characteristics of Electrical Discharges in Magnetic Fields*, National Nuclear Energy Series I-5, (McGraw-Hill, 1949).
12. J. R. PIERCE, J. Appl. Phys., **11** (1940), 548.
13. C. E. BERRY, R. S. I., **27** (1956), 849.
14. C. P. KEIM, Nature, **175** (1955), 98.
15. J. KOCH, Nature, **161** (1948), 566.
16. J. BERGSTRÖM, Arkiv f. Fysik, **5** (1952), 191.
17. S. THULIN, Arkiv f. Fysik, **9** (1955), 107.
18. K. O. NIELSEN, *Electromagnetically Enriched Isotopes and Mass Spectrometry*, (Edited by M. L. Smith, Butterworths Scientific Publications, London, 1956).